IEEE Access
Multidisciplinary | Rapid Review | Open Access Journal

Received November 4, 2020, accepted November 10, 2020, date of publication November 16, 2020,
date of current version November 25, 2020.

Digital Object Identifier 10.1109/ACCESS.2020.3038111

High Performance Hybrid Piezoelectric-Electromagnetic Energy Harvester for Scavenging Energy From Low-Frequency Vibration Excitation

YUN YANG[1,3], TINGTING CAI[2], SHUPING XUE[1], XIAOGUANG SONG[1], AND XINAI CUI[1]

[1]Department of Mining Engineering, Luliang University, Lvliang 033000, China
[2]Department of Chemistry and Chemical Engineering, Luliang University, Lvliang 033000, China
[3]School of Instrument and Electronics, North University of China, Taiyuan 030051, China

Corresponding author: Tingting Cai (dbdxctt@163.com)

This work was supported in part by the Scientific and Technological Innovation Programs of Higher Education Institutions in Shanxi (STIP) under Grant 2019L0953 and Grant 2019L0942, in part by the Science and Technology Planning Projects, Lvliang, under Grant GYZDYF2019081 and Grant 2020SHFZ36, in part by the Key Laboratory of Maintenance and Inspection of Coal Mine Mechanical Equipment of Lvliang City, China, and in part by the Key Innovation Team for Fault Diagnosis and Health Management Technology of Coal Mine Machinery Equipment of 1331 Project in Shanxi Province under Grant TD201812.

ABSTRACT There are many difficulties in the power supply of the wireless monitoring system for coal mine mechanical equipment. Vibration energy scavenging is a green and effective way to solve this problem considering the intense and continuous vibration of coal mechanical equipment. In this paper, a novel hybrid vibration energy harvester was designed and manufactured, which combined electromagnetic and piezoelectric transduction units. Vibration drives the two units to move in the vertical and horizontal directions to realize the energy conversion. The mathematic model was built to calculate and predict the performance while the simulation on the distribution of magnetic field and piezoelectricity potential provided the details in the design. Besides, the output signal generated by the vibration excitation of the electromagnetic unit, piezoelectric unit and the whole energy harvester were studied simultaneously. Moreover, the resonance frequency was tested to be 14Hz, and the optimum matching impedance was measured to be 1kΩ and 10kΩ with the parallel and series connection of PH and EH, respectively. The maximum output power of the HPEH with the parallel connection pattern can reach 80.10mW at the acceleration of 2g. In the application experiment, the HPEH can facilely light up 120 LEDs and supply stable power for the electronics and sensors.

INDEX TERMS Vibration energy acquisition, hybrid energy harvester, electromagnetic, piezoelectric, coal mine mechanical equipment.

I. INTRODUCTION

Coal plays a significant role in economic development and industrial production as a primary energy in the world. The safety and reliability of coal mechanical equipment is the foundation to ensure the production efficiency and economic benefits of the coal mine. Employing wireless sensor network [1] to monitor the signal of coal mechanical equipment such as the vibration and temperature in real-time is an effective way to discover the equipment failure. However, there are many difficulties in the power supply of the remote places in the coal mine. Firstly, long-time operation in the harsh environment with rotation, strong vibration tends to cause the ageing and damage to the power supply cable. Moreover, if the battery is adopted for power supply, it must be sealed in the monitoring system to eliminate the safety problems like the electric spark, and it brings another headache that how to replace it frequently. While the large equipment in the coal mine like drum rock cutting vibrator in shearer often contains large amounts of energy with a vibration frequency band of 1-200Hz and acceleration concentrated lower than 5 g [2]. Therefore, it is a desirable strategy to harvest vibration energy from the equipment and convert it to the continuous supply power for the monitoring system considering the intensive and continuous vibration of the mechanical equipment.

The associate editor coordinating the review of this manuscript and approving it for publication was Diego Masotti.

Vibration-driven environmental energy harvesting technology uses energy-converting devices to convert environmental energy into electrical energy for output. At present, vibration-driven energy harvesting technologies mainly include piezoelectric [3]–[10], electrostatic [11], electromagnetic [12], magnetostrictive [13] and triboelectric [14], [15]. Nevertheless, these reported vibration energy harvesters still face some problems in practical application [16], [17] such as large energy dissipation rate, narrow vibration response range, and low energy conversion efficiency. Recently, the research on hybrid vibration energy harvesters (HVEHs) provides a novel method to improve the efficiency of vibration harvesting.

Among the HVEHs, the hybrid piezoelectric and electromagnetic harvesters (HPEHs) in numerous studies have demonstrated their superiority in the structural design and the improvements in the output power and voltage. The individual piezoelectric and electromagnetic vibration harvesters are both widely researched, the former generates large power density and high voltage [18] while the latter produces higher energy conversion efficiency and high power [19]. Besides, they all bring sustainable energy output without any pollutants attached [20] and suitable for application in multiple environments. HPEHs can combine both the advantages of them through proper configurations design and optimize the parameters related in the structure. Xia *et al.* [21] conducted numerical simulations on an HPEH with different electrical boundary conditions to predict the output of the HPEH and help to optimize the structure. Xu *et al.* [22] fabricated a mesoscale HPEH prototype and compared with a stand-alone piezoelectric energy harvester and a single electromagnetic energy harvester. The results showed a higher peak and wider bandwidth wave of the output power and agreed well with the theoretical values.

The output performance of the HPEHs was also reported in many kinds of literature. Li *et al.* [20] found that the hybridization scheme lowers the peak power by more than half compared to the piezo-only case. However, total power output increased by more than ten times, and 99 LEDs was lighted up due to the piezoelectric and electromagnetic coupling effect. Fan *et al.* [23] reported an HPEH with the size of 75 mm×36mm×16mm that can scavenge energy from both low-frequency and bi-directional excitations. The power of the PH and EH on the sinusoidal excitation of 1.5g can reach 0.28mW and 1.42mW simultaneously while it can light up 42 LEDs. Iqbal *et al.* [24] reported a hybrid vibration and wind energy harvester of 85mm×80mm×40mm. At the acceleration of 0.4g and 0.6g, the power achieved were 0.156mW and 2.214mW. Tadesse *et al.* [25] brought up a design of HPEH with the size of 25 mm×30 mm×125mm, while the power achieved by PH and EH were respectively 0.02mW and 25mW. Toyabur *et al.* [26] mentioned a multimodal HPEH for low-frequency ambient vibrations of 12-22 Hz, the parameters of the size were 105 mm×30 mm×20mm and the power of PH and EH were both 0.25mW which can supply electricity for humidity and temperature sensors. Lin *et al.* [27] presented a hybrid power generator composed of a 36mm×17mm×0.73mm piezoelectric cantilever and a 40 mm long electromagnetic tube. The power of 2.173mW at 25 Hz of 1 g was got, which was higher than that of a single piezoelectric or electromagnetic generator of the same dimensions.

In this paper, we proposed a novel HPEH to scavenge the vibration energy from the coal mine mechanical equipment. Under the excitation of low-frequency vibration of 14Hz, the maximum output power of 80.10mW was achieved. The HPEH with rectifier and charging circuit can light 120 light-emitting diodes (LEDs) and drive the common-used sensors and electronics to work continuously, which was more effective compared with the previously reported HPEHs and indicated the potential applications in power supply for low-power monitoring equipment. Moreover, the protective cylindrical shell was indurative, and the design of shape and structure can provide secure space for the sensors such as acceleration and temperature sensors to integrate with the HPEH as a self-powered monitoring system for the mechanical equipment and equipment in the coal mine.

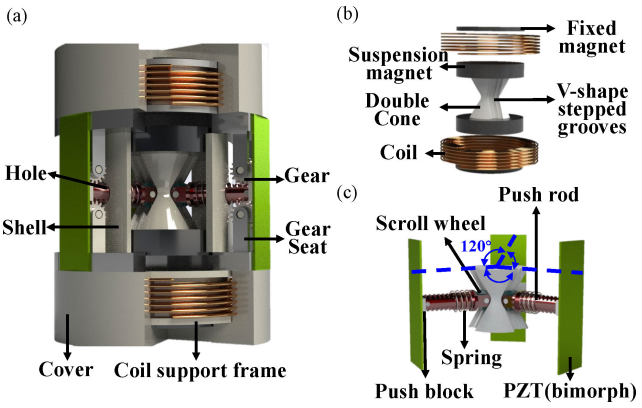

FIGURE 1. The schematic diagram of the proposed HPEH. (a) The whole structure and cross-section drew of the HPEH (b) The EH unit (c) The PH unit.

II. CONFIGURATION AND PRINCIPLE SIMULATION OF THE PROPOSED HPEH

A. THE STRUCTURE AND PROTOTYPE FABRICATION

The proposed HPEH has an approximately cylindrical appearance of longitudinal symmetry, as schematically illustrated in Fig. 1a. The size of the device is Φ 83mm×117mm, and it weighs 537g. The structure of the outer layer is simple, two copper coils and two magnets are fixed in the covers while three piezoelectric plates are inserted in the two covers and outside the shell. The coils are fixed in the coil support frame that inside the cover and 2mm apart from the middle suspension magnets, which are determined by simulation calculation of the magnetic field. An interference fit is adopted between the coil support frame and the upper cover. Inside the shell is the motion structure with a double circular cone as the key transmission component.

The whole HPEH is composed of two units, an electromagnetic harvester (EH), and a piezoelectric harvester (PH).

TABLE 1. Structural parameters of the proposed HPEH.

Component	Parameter	Value
3D printed parts	Shell	Φ83mm×117mm
	Bipyramid cones	Φ29.16mm/1.4×30mm
	Push rod	Φ0.85mm×35.2mm
Copper coil	Internal diameter	Φ54mm
	External diameter	Φ70mm
	Height	14mm
	Wire diameter	0.1mm
Spring	Diameter	Φ1mm
	Height	15mm
	Wire diameter	0.2mm
Nd-Fe-B magnet	Fixed magnet	Φ50.0mm×3.0mm
	Suspension magnet	Φ50.0mm×10.0mm
	Young's module	41.4×10^9 Pa
	Density	7.4×10^3 kg/m^3
	Poisson	0.28
PZT piezoelectric plates	Size	60mm×20mm×0.1mm
	Elastic modulus	110×10^9 Pa
	Density	7.6×10^3 kg/m^3
Substrate	Elastic modulus	140×10^9 Pa
	Density	8.26×10^3 kg/m^3

The EH (Fig.1b) is composed of four magnets and two copper coils which are distributed longitudinally symmetrically. Therein, two of the fixed magnets has mentioned above, while the other two stick to the ends of the double circular cone to form the sandwich-shaped suspension magnet unit. For the PH unit, the main component is the double circular cone in the center. Around it are three push rods and corresponding piezoelectric plates that distribute at an angle of 120 degrees, as shown in Fig. 1c. Each push rod connects the motion of the double cone and the piezoelectric plate through the hole in the shell, with a scroll wheel at one end and a push block at the other end. There are three V-shape stepped grooves on the surface of the double cone, which are used as the rolling track of the scroll wheel. When the double cone moves up and down, the scroll wheel will roll in the V-shape stepped groove of the double cone, transforming the vertical motion of the double cone into horizontal motion of the push rods. The push block at the other end of the push rod can push the piezoelectric plate and cause deformation. In this way, the motion position transforms from EH to PH unit.

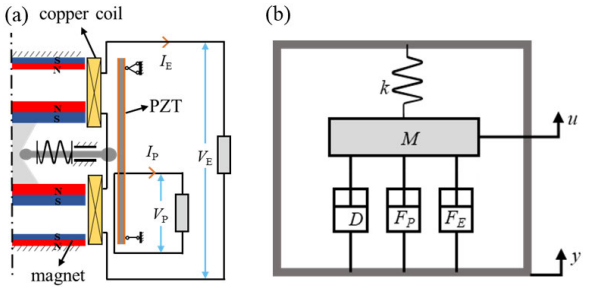

FIGURE 2. (a) Schematic diagram of the HPEH and (b) the equivalent SDOF system.

In order to realize the smooth linear motion of the push rod, rack structure is adopted, and the teeth are engraved on the upper and lower sides of the push rod. Moreover, the two gears are set just outside the hole, between the shell and the piezoelectric plate. The springs wrap the push rod to assistant the automatic restoration of the push rod to its original position during the motion. The piezoelectric plates are fixed by inserting the reserved gap in the upper and lower covers with a simply supported beam structure. This structure is convenient for fixing and replacing of the piezoelectric plates, while it is strong and rigid enough. The whole process can be divided into four stages which can be found in Fig. 4a.

The primary supporting frameworks including the double circular cone, shell, two covers at the top and bottom, were designed and printed in our laboratory with the FDM (fused deposition method) 3D printer and the primary print material used was PLA (polylactic acid). In contrast, the push rods with teeth were printed with nylon considering its high strength and durability requirement. The magnets in the EH unit are the Nb-Fe-B permanent magnets, and the material of the coil is copper. The PZT dual piezoelectric plates used in the PH is commercially available, which consist of piezoelectric bimorph (PZT-5H) and substrate (Fe-Ni42 alloy). Moreover, screws of high precision were purchased to connect the upper and lower cover and the shell in the middle. While the bearings, springs were also bought. The detailed information of the components is shown in Table 1.

B. MATHEMATICAL MODELLING AND ANALYSIS OF THE PROPOSED HPEH

The HPEH is composed of two submodules. One is the electromagnetic unit composed of suspension magnets and copper coils. The other is the piezoelectric unit formed by the simply supported beam of the piezoelectric plate as shown in Fig. 2a. It can be modelled as a vibration system with a single degree of freedom (SDOF) as shown in Fig. 2b, which consists of the modal mass M, the spring stiffness K, the damping coefficient D, and the restoring force F_P and F_E induced by the EH. More specifically, M refers to the sandwich-shaped suspension magnet unit, which consists of two magnets and the double circular cone between them. K is the equivalent mechanical spring stiffness of the system that

determined by the magnetic force, the spring restoring force on the push rod and the deformation restoring force of the piezoelectric plate at the condition of open-circuit state of both PH and EH. D is the equivalent mechanical damping of the whole system under open-circuit conditions of PH and EH, and it was caused by all the frictional loss of the moving components.

F_P is the restoring force caused by the voltage generated by the PH, and its magnitude is related to the force-voltage factor α and the output voltage V_P of the PH, which can be expressed by (1). F_E is the restoring force due to the current generated in EH, and its value is related to the force-current factor β and the induced current I_E of the induction coil, which can be expressed by (2).

$$F_P = \alpha V_P \tag{1}$$

$$F_E = \beta I_E \tag{2}$$

Then, the motion differential equation of the electromechanical system is given by (3), where u is the relative displacement of the internal centre magnet of the harvester [28]. The relation between the piezoelectric voltage V_P and the piezoelectric current I_P is given by the electric boundary condition (4) of the PH. The relationship between coil current I_E and load voltage V_{EL} is represented by the electric boundary condition (5) of the EH [29].

$$M\ddot{u} + D\dot{u} + Ku = F - \alpha V_P - \beta I_E \tag{3}$$

$$I_P = \alpha\dot{u} - C_P\dot{V}_P \tag{4}$$

$$V_{EL} = \beta\dot{u} - rI_E - L_C\dot{I}_E \tag{5}$$

The symbols and definitions in the equations were shown in Table 2.

TABLE 2. Experimental parameters identification and the value.

Parameter	Symbol	Value	Unit
Mass	M	270.8	g
Damping coefficient	D	5.183	Ns/m
Spring stiffness	K	2095.39	N/m
Natural frequency	f_n	14	Hz
Piezoelectric force-voltage factor	α	1.334×10^{-3}	N/V
Electromagnetic force-current factor	β	77.27	N/A
Piezoelectric clamped capacitance	C_P	78.83	nF
Coil resistance	r	2.26	kΩ
Coil inductive	L_C	1.30	H

The energy balance equation (6) of the system can be obtained by multiplying (3) by the relative velocity $\dot{u}$ and then integrating with time. The results showed that the input mechanical energy was converted into kinetic energy, potential energy, mechanical damping loss and transducers acquired energy. Besides, the energy obtained from the PH can be subdivided into three parts: the electrostatic energy stored in the clamp capacitance, the energy obtained through the acquisition interface circuit, and the energy loss due to the inherent resistance, as shown in (7). Similarly, the energy obtained by EH can be divided into three parts: the electromagnetic energy stored in the coil's inductance, the dissipation caused by coil resistance and the energy obtained by the acquisition interface circuit, as shown in (8) [21].

$$\int F\dot{u}dt = \frac{1}{2}M\dot{u}^2 + \frac{1}{2}Ku + \int D\dot{u}dt + \int \alpha V_P\dot{u}dt + \int \beta I_E\dot{u}dt \tag{6}$$

$$\int \alpha V_P\dot{u}dt = \frac{1}{2}C_P V_P^2 + \int V_P I_P dt \tag{7}$$

$$\int \beta I_E\dot{u}dt = \frac{1}{2}L_C I_E^2 + \int rI_E^2 dt + \int V_{EL}I_E dt \tag{8}$$

There is a coupling relationship between the two submodules of HPEH. Suppose the basic acceleration is $a = a_M \sin\varpi t$, where a_M is the amplitude, and ω is the angular frequency. In general, the PH and EH loads are treated as two pure resistances R_P and R_E, respectively. Then the electric boundary conditions (4) and (5) can be rewritten in terms of (9) and (10). (11) and (12) can be obtained through the Laplace transform of (9) and (10) under zero initial conditions.

$$\alpha\dot{u} = \frac{V_P}{R_P} + C_P\dot{V}_P \tag{9}$$

$$\beta\dot{u} = (r + R_E)\, I_E + L_C\dot{I}_E \tag{10}$$

$$V_P(j\varpi) = \frac{j\varpi\alpha R_P}{j\varpi R_P C_P + 1} U(j\varpi) \tag{11}$$

$$I_E(j\varpi) = \frac{j\varpi\beta}{j\varpi L_C + (r + R_E)} U(j\varpi) \tag{12}$$

The power collected from PH and EH is equal to the power dissipated on the load resistance R_P and R_E, respectively. It can be calculated by (13) and (14) according to the relative displacement u_M. The power of HPEH can be regarded as the sum of the power collected from PH and EH, which can be calculated by (15).

$$P_{PH} = \frac{1}{2R_P}|V_P(s)|^2 = \frac{u_M^2}{2}\frac{\varpi^2\alpha^2 R_P}{\varpi^2 R_P^2 C_P^2 + 1} \tag{13}$$

$$P_{EH} = \frac{R_E}{2}|I_E(s)|^2 = \frac{u_M^2}{2}\frac{\varpi^2\beta^2 R_E}{\varpi^2 L_C^2 + (r + R_E)^2} \tag{14}$$

$$P_{HPEH} = \frac{u_M^2}{2}\left[\frac{\varpi^2\alpha^2 R_P}{\varpi^2 R_P^2 C_P^2 + 1} + \frac{\varpi^2\beta^2 R_E}{\varpi^2 L_C^2 + (r + R_E)^2}\right] \tag{15}$$

By substituting $F = -Ma$, (11) and (12) into the Laplace transform of (3), the transfer function (16) between relative displacement $U(\varpi j)$ and input acceleration $A(\varpi j)$ is obtained.

$$\frac{U(\varpi j)}{A(\varpi j)} = \frac{-M}{-\varpi^2 M + j\varpi D + K + \frac{j\varpi\alpha^2 R_P}{j\varpi R_P C_P + 1} + \frac{j\varpi\beta^2}{j\varpi L_C + (r + R_E)}} \tag{16}$$

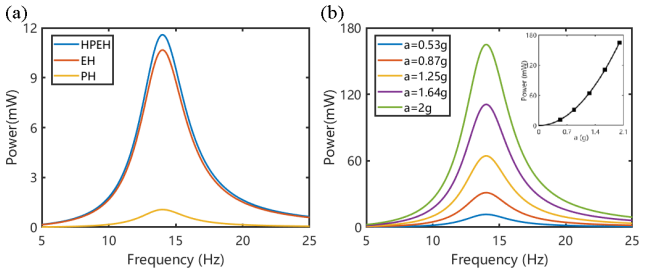

FIGURE 3. Simulation of the influence of external excitation (a) frequency (b) acceleration on the output power of HPEH, EH and PH. (The inset shows the increasing trend of the output power of the HPEH with the change of the acceleration.)

By combining (15) and (16), the power of HPEH can be obtained and given by (17).

$$P_{HPEH} = \frac{1}{2}M^2 a_M^2 \frac{\frac{\alpha^2 R_P}{\varpi^2 R_P^2 C_P^2+1} + \frac{\beta^2 R_E}{\varpi^2 L_C^2+(r+R_E)^2}}{Q_{Im}^2 + Q_{Re}^2} \tag{17}$$

Therein:

$$Q_{Im} = D + \frac{\alpha^2 R_P}{\varpi^2 R_P^2 C_P^2 + 1} + \frac{\beta^2 (r + R_E)}{\varpi^2 L_C^2 + (r + R_E)^2}$$

$$Q_{Re} = \frac{K}{\varpi} - \varpi M + \frac{\varpi \alpha^2 R_P^2 C_P}{\varpi^2 R_P^2 C_P^2 + 1} + \frac{\varpi \beta^2 L_C}{\varpi^2 L_C^2 + (r + R_E)^2}$$

In the mathematical model, the modal mass M, coil resistance r, coil inductance L_C, piezoelectric clamper capacitance C_P can be directly measured. Other system parameters can be obtained by using resonance frequency scanning, free attenuation vibration method and corresponding calculation formula. The test process and calculation formula of model parameters were in the Supplementary information. All the model parameters are listed in Table 2.

According to (17) and system parameters in Table 2, the influence of external excitation parameters such as vibration frequency and acceleration on output power can be simulated, as shown in Fig. 3. It can be seen from Fig. 3a that the output power of HPEH is greater than that of EH and PH under excitation conditions of different frequencies. HPEH can obtain the maximum output power under the excitation of the resonant frequency of 14Hz and the resonance frequencies of HPEH, EH and PH are consistent. Fig. 3b shows that the higher acceleration can generate higher output power and the increased speed becomes faster with the acceleration rising, like the shape of a parabola as shown in the inset, which is the feature of a quadratic polynomial.

C. THE MECHANISM ANALYSIS OF THE MOTION AND ELECTRICITY GENERATION

The HPEH makes periodic motions when excited by vibration, and the power generation process involves four steps. When external vibration occurs, the floating magnet units will make up-down vibration near the equilibrium position due to the double action of magnetic repulsion and gravity. According to the law of Faraday electromagnetic induction, the upper

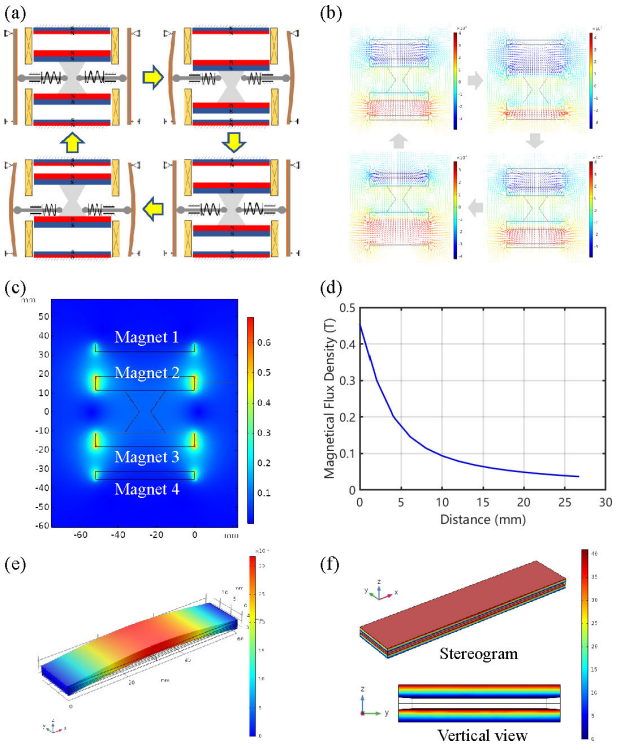

FIGURE 4. a) The movement mechanism of the four principle steps b) The simulation of the magnetic field of the EH in a vibration period c) The magnetic flux density distribution of the four magnets in equilibrium state d) The curve of the magnetic flux density at different distances from Magnet2 e) The strain distribution map at the limited position of half the piezoelectric bimorph f) Potential distribution of piezoelectric beam at the maximum displacement of the piezoelectric plates from two directions.

and lower coil will both generate induced electromotive force by cutting the magnetic induction line. Then the two coils are connected to lead the current out. When excitation actuates the vibration of suspended magnet unit, it immediately drives the movement of the double cone, then forcing the push rods with the pulley to roll along the V-shaped stepped groove and constantly changing the relative position on the double cone, so the three piezoelectric beams will be triggered to vibrate periodically by the push rods via the mechanical contact caused by the gear-rack drive. According to the principle of the piezoelectric effect, rearrangement occurs inside the piezoelectric ceramic crystal because of the periodic reciprocating motion under the impulse of pressure, thereby generating an induced potential between the two electrodes of the piezoelectric plate. Considering the motion state of the three piezoelectric beams are synchronous, they are connected in serial connection to obtain the total potential of the PH.

To prove the feasibility of this structure, COMSOL Multiphysics 5.2a software was used for simulation analysis. The magnetic field distribution in the four steps was simulated (Fig. 4a). From the distribution of the arrow color, it can be speculated that the stronger magnetic induction lines are mainly located inside the cylinder. Meanwhile, the magnetic field strength gradually decreases outside the central position. From the perspective of the arrow length and density,

the greater magnetic field strength is near the middle magnet unit because of the two magnets in the suspension magnet unit. Considering the arrow direction, the horizontally distributed magnetic induction lines are closer to the fixed magnets and change with the vibration-caused position of the suspend magnet unit. Fig. 4c shows the simulation results of the magnetic flux density distribution of the four magnets. Taking "Magnet 2" as an example, the curve of the relationship between the magnetic flux density and the distance from the magnet was provided. As shown in Fig. 4d, when the distance varied from 0 to 5mm, the magnetic flux density changed greatly. Therefore, the coil should be arranged as close as possible to the magnet. On the other hand, when the magnet is vibrating, a certain movement space should be reserved on both sides of the magnet to prevent the magnet from getting stuck or hitting the side wall frequently due to machining and assembly accuracy. Therefore, in the horizontal position, we place the coil 2 mm from the magnet.

Moreover, the potential distribution on the PZT piezoelectric sheets was analyzed, and the performance of the device was assessed. In the HPEH, three piezoelectric plates were distributed with an angle of 120 degrees between each other, and the force point is in the middle of the piezoelectric sheets. Due to the limited bending distance and fast recovery speed of the piezoelectric plates, the service life of the simple beam structure can extent immensely compared to the cantilever beam structure. Fig. 4e displays the strain distribution map at the limited position of half the piezoelectric bimorph with the vibration excitation. Because of the simple-supported beam structure, the two ends of the piezoelectric plates are immovable in the z-direction, so the maximum distance located at the position where the putter touches. In the balance position, the electric charge is evenly distributed in the whole piezoelectric plates. When deformation appears, the piezoelectric effect results in the redistribution of the electric charge, causing the voltage difference between the two surfaces (Fig. 4f) and the maximum voltage emerge where the push rod touches. To achieve the maximum open-circuit voltage and power, the three piezoelectric sheets are connected in series [30].

III. EXPERIMENTAL STUDIES AND DISCUSSION

A. EXPERIMENT SETUP

In order to verify the effectiveness and examine the performance of the designed HPEH, the experimental platform was constructed, as shown in Fig. 5. The examination system was composed of a signal generator (SA-SG030, SHIAO), a power amplifier (SP-PA020, SHIAO), a vibration exciter (SA-JZ010, SHIAO), an accelerometer (UT315, UNI-T) and an oscilloscope (MSO2024B, Tektronix). Among them, the first three devices constituted the excitation system which can provide vibration excitation with different frequency and acceleration for the energy harvester. The accelerometer fixed on the vibration exciter can test the vibration state of the exciter. When the external periodic vibration was applied, the corresponding periodic electricity signal displays on the oscilloscope screen and the data can be saved and analyzed by the connected computer. In addition to the above mentioned, a rectifier-filter circuit board, loaded with resistances and capacitors was also needed to transform the generated electricity from AC to DC.

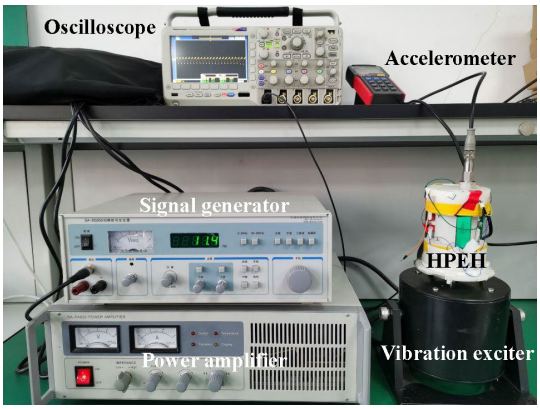

FIGURE 5. The test platform of HPEH.

B. THE OUTPUT OF EACH PART OF EH AND PH UNIT

There are two electricity generation modules in the proposed HPEH, each of them is composed of several units, so it is of great necessity to study the synergistic effect of them.

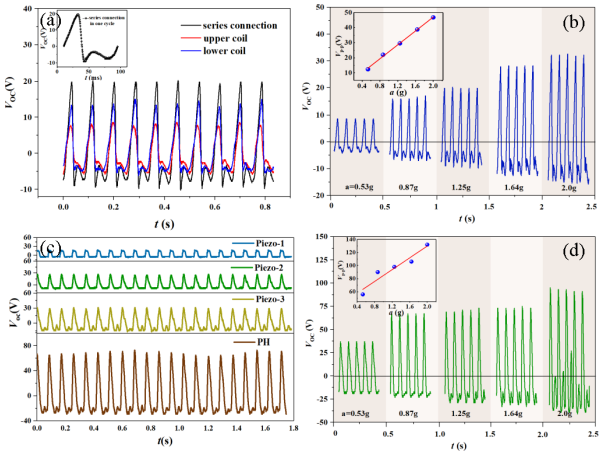

FIGURE 6. Oscilloscope voltage waveforms of the EH unit and PH unit a) the two coils and the whole EH (The inset shows the waveform of EH in one cycle) b) the EH under different vibration acceleration (The inset shows the relationship between the voltage and acceleration) c) the three piezoelectric plates and the whole PH d) the PH under different accelerations(The inset shows the relationship between the voltage and acceleration).

As shown in Fig. 6a, the output of the two coils in the EH reveals identical waveform period when the vibration frequency is 14 Hz and the acceleration is 1.25g, but the peak values do not coincide. The peak-to-peak voltage (V_{p-p}) of the lower coil is about 1.5 times than that of the upper coil, which is different compared with the simulation results. This phenomenon attributes to the deviation in the HPEH assemble. Also, although the positions of the two coils and

the fixed magnets are designed to be symmetrical, the equilibrium position of the suspension magnet unit stays lower than the geometric center due to the gravity. Therefore, when the vibration loaded, the downward distance exceeds the upward, resulting in the higher peak of the lower coil. Since the two coils are connected in series, the voltage amplitude of the whole EH is larger than both of them. Meanwhile, the inset of Fig. 4a shows the detailed waveform in one cycle, the alternating voltage signal is not symmetric for the same reason above. The voltage waveforms under different vibration acceleration conditions are illustrated in Fig. 6b. The V_{p-p} increases linearly with the gradually increasing acceleration value and the coefficient of determination (R^2) is 0.99, indicating a high degree of linearity.

Three piezoelectric beams are arranged on the periphery of the HPEH, and the voltage curves of them are tested. Under the vibration of 14 Hz and 1.25g, the three waveforms exhibit the same cycle and changing trend (Fig. 6c), which is consistent with the structure principle. However, the V_{p-p} of the three piezoelectric plates are different, this may be due to the insufficient assembly accuracy and the uniformity of the PZT materials. When connected in series, a combined voltage waveform is achieved, and the peak-to-peak value becomes much higher. Besides, the voltage waveform of the series connection is recorded under different acceleration conditions, and the V_{p-p} rises with the increasing of the acceleration (Fig. 6d), showing a linear trend approximately ($R^2 = 0.92$).

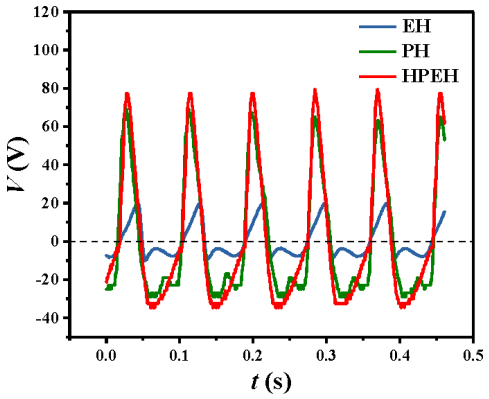

FIGURE 7. Voltage waveforms of the EH unit, PH unit and the HPEH under the vibration of 14 Hz and 1.25g.

As can be seen from Fig. 6a and c, the frequency of each output unit is consistent, and the output voltage of each unit can be directly superposition in series without rectifier module, which is of great convenience for subsequent analysis and application. This phenomenon can be attributed to the transmission structure of the harvester, which makes the electromagnetic and piezoelectric units vibrate synchronously. Moreover, the phase of the EH, PH and the whole HPEH was also recorded by the oscilloscope and exhibited the synchronization in the frequency and phase position, which is shown in Fig.7.

C. VOLTAGE RESPONSES FROM FREQUENCY SWEEPS

Since the vibration frequency of the output voltage of the electromagnetic unit and the piezoelectric unit are identical, the electromagnetic and piezoelectric parts can be connected in series to study the total output voltage or each of them.

The resonance frequency corresponds to the maximum output, so in order to improve the vibration energy acquisition efficiency, the frequency response range of EH, PH and HPEH were tested separately. The test frequency range was chosen as 7-80 Hz since we focused mainly on the low-frequency vibration harvest.

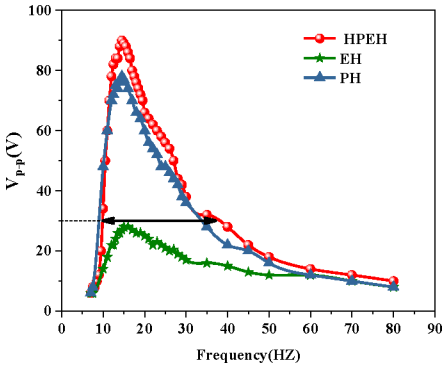

FIGURE 8. The peak-to-peak output voltage of HPEH, EH and PH at different vibration frequencies.

According to the curve in Fig.8, the resonance frequencies of the two units are all around 14 Hz, which is consistent with the whole HPEH. Meanwhile, the result is conformed well to the results in the mathematical modelling calculation. Moreover, the V_{p-p} of the HPEH is above 30V in the range of 10-37Hz, which shows a relatively wide response frequency band. While when the resonant frequency is around 14 Hz, the V_{p-p} even reaches 90V. An obvious distinction of V_{p-p} appears between EH and PH, which can be indicated that the voltage of HPEH is mainly affected by the PH unit.

D. IMPEDANCE MATCHING AND OUTPUT POWER

The change law of the output voltage and power under different load resistances were studied with the rectifier-filter circuit to convert the periodically AC to DC and the capacitors to be charged and store the electrical energy to power the load. A wide range of the load resistance value of 10-$10^7\Omega$ was applied, and the vibration frequency and acceleration were set as 14 Hz and 0.53g respectively.

The whole HPEH is composed of two parts, PH and EH, and the connection pattern of them can significantly influence the output signal of the HPEH. Therefore, the different performance with the parallel and series connection patterns was also studied with the different rectifier-filter circuits shown in Fig. 9a,b.

The results in Fig. 9c show that with the increase of the resistance value, the voltage of the EH and PH are both increasing, but there are differences in detail. For the EH, it starts to rise at a low resistance value, and the rise trend

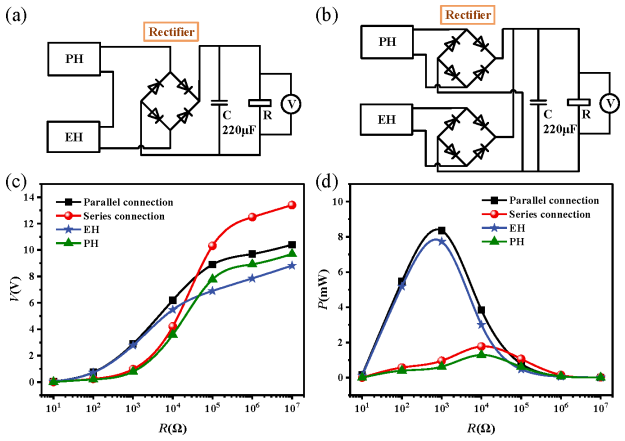

FIGURE 9. The two connection circuits of PH and EH (a) series and (b) parallel connection; The effect of load resistance on the (c) partial voltage and (d) output power of EH, PH and HPEH in series connection and parallel connection respectively.

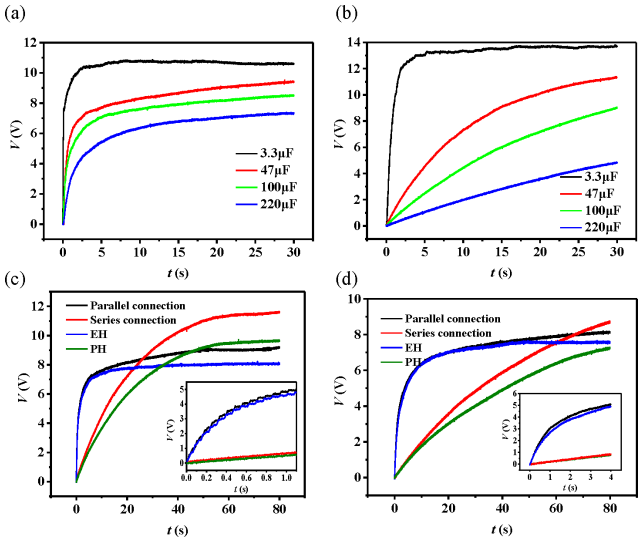

FIGURE 10. The charging voltage curve of the four different capacitors in two patterns of (a) parallel pattern (b) serial pattern; The charging voltage curve of the EH, PH, the parallel connection, the serial connection of two capacitors (c)100μF and (d) 220μF.

slows down after 10kΩ. While for the PH unit, an obvious increase appears at about 100Ω and nearly reaching the peak value at $10^5\Omega$, and the change rate at 10^6-$10^7\Omega$ is not significant. For the parallel connection, the variation tendency is similar to the EH with a slightly higher voltage value. While the voltage trend of the series connection is mainly determined by the PH unit, and the voltage reach 13.4V at $10^7\Omega$.

$$P = \frac{U^2}{R} \tag{18}$$

The output power of the HPEH was calculated according to the Ohm's Law shown in equations (18) (U refers to voltage, R refers to resistance, and P refers to power). The relationship between the output power and the load resistance is shown in Fig. 9d. The EH and PH exhibit a tremendous distinction, such as the maximum value of EH appeared at 1kΩ, and the other appears at 10kΩ. Moreover, the output power of the EH is much higher than that of PH. As for the whole HPEH, similarly, the trend of the parallel and series connection resembles EH and PH respectively, and the maximum output power of them was approximately the same with the individual EH and PH. Notably, the maximum output power 8.35mW of the HPEH is achieved at 1kΩ, which mainly depend on the EH, other than the voltage results.

E. EFFECT OF CAPACITANCE AND ACCELERATION ON THE OUTPUT VOLTAGE AND POWER

The capacitor charge response was also a significant parameter for the harvester's power generation. In order to study the relation of the capacitance with the connection pattern, the test was carried out with two at the acceleration of 0.63g and vibration frequency of 14Hz. As can be seen from Fig.10a and b, when charging capacitors of different capacitance, the growth rate of both the parallel and the series connection were slower with the increase of the capacitance value. Also, the parallel pattern can charge the capacitors more quickly, while the serial connection can charge the capacitor to a higher voltage. To further analyze the performance to charge capacitors, the voltage charging curves of capacitors of 100μF and 220μF were measured and drawn in different connection method as shown in Fig.10c and d. For the two capacitors, at the beginning, thus before 26.25s and 67.71s, the voltage value of the parallel connection is higher. However, the capacitors were charged to 11.59V and 8.69V respectively of the serial connection at the 80s. Meanwhile, the parallel connection was 9.20V and 8.15V respectively.

Generally, the embedded sensors of the mechanical condition monitoring system in the coal mine are working at the voltage of 3.3V or 5V, so the two connection patterns can both meet the requirements. As can be seen from the inset of Fig. 10c and d, when the capacitors of 100μF and 220μF are charged to 5V, only 1.1s and 3.79s are needed respectively in parallel, while the serial connection only reaches 0.78V and 0.73V in such short time. Therefore, the parallel pattern is a better choice in the practical test.

In order to explore the influence of vibration acceleration on output electricity of the proposed HPEH in the presence of resistance load, the output voltage and power under different vibration intensity was examined at a series of accelerations: 0.53g, 0.87g, 1.25g, 1.64g, and 2.0g. The test frequency was 14Hz, and the load resistance of the parallel and series connection was 1kΩ and 10kΩ, respectively, which is achieved in the previous test as the optimum matching resistance. As can be seen from Fig. 11, both the output voltage and power increase with the growing acceleration and the trend was almost linear. With the acceleration of 2.0g, the output power can reach 80.10mW and 23.10mW respectively in the parallel and series connection, displaying a great potential to power electronics and sensors. The variation trend of the power with the parallel connection has the same parabolic

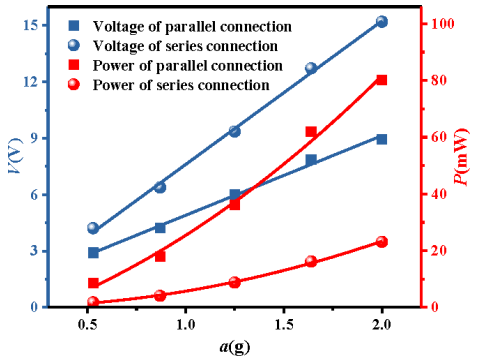

FIGURE 11. The trend of the output voltage and power under different vibration acceleration.

shape like the simulated results in the mathematic model in Fig.3b. Therefore, the parallel connection was adopted in the application experiment.

F. THE APPLICATION OF HPEH IN THE POWER SUPPLY FOR ELECTRONICS AND SENSORS

Accordingly, we assembled rectifier-filter circuits (Fig. 12b,f) with the capacitor of 220μF to gain DC and storage electricity to the capacitor and power the LEDs, multi-purpose electronic sensors, electronic thermometer and electronic clock.

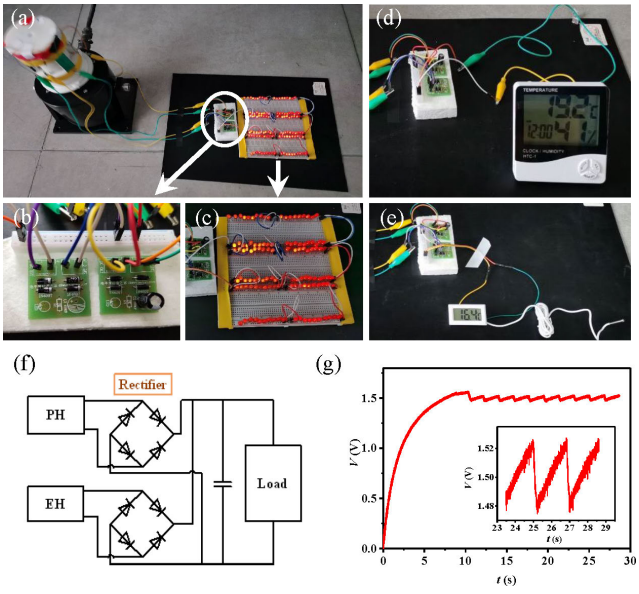

FIGURE 12. a) The powering test system b) The rectifier-filter circuit board c) The lighted LED array d) HPEH powering the multi-purpose electronic sensors e) HPEH powering the electronic thermometer f) Schematic diagram of the rectifier-filter circuit g) The charging characteristics of the storage capacitor while the electronic thermometer is in operation.

We connected 120 commercial LEDs on a breadboard in parallel which forms a 10 × 12 array and imposed a vibration excitation with an acceleration of 0.87 g and frequency of 14 Hz onto the HPEH. The LEDs were of 5 mm in size and red color when lighted, and the basic and maximum forward voltages were 1.45 V and 1.65 V, respectively. When external vibration began, LEDs will all be lighted up with bright light (Fig. 12a and c, Video 1). Furthermore, we investigated the charging performance of the HPEH, and the results showed that it could provide stable electricity for electronics and sensors. The household multi-purpose electronic sensors (Fig. 12d, Video 2) and the electronic thermometer (Fig. 12e) can be powered to work continuously and steady with the vibration of 0.88 g and 14 Hz. Moreover, the electronic clock can keep operation for nearly 2 minutes after charging for only 10 seconds at the vibration frequency of 14 Hz and the acceleration of 0.63g (Video 3).

Fig.12g showed the voltage change of the capacitor in the rectifier-filter circuit when HPEH provided stable power for the thermometer. In the first 10s, HPEH charged the capacitor to 1.6V. Then the thermometer was plugged into the circuit and turned on, and the voltage of the capacitor dropped to 1.48V simultaneously. Subsequently, a sawtooth waveform was formed and remained stable between 1.48V and 1.53V during the whole period of the power supply for the thermometer. The videos attached in the Supplementary information showed the actual process of how the experiment was conducted. The experiment results were powerful proof for the promising application of HPEH as the substitute for the power supply of the unattainable monitoring system of the mechanical equipment in the coal mine and other similar condition.

IV. CONCLUSIONS

In this paper, we proposed a novel design of hybrid harvester for the vibration energy harvest, which is comprised of piezoelectric and electromagnetic transduction units. The key component of the double circular cone can transform the vibration of the EH in the vertical direction to horizontal vibration of the PH coupled with the stepped grooves on the surface and the scroll wheel at one end of the push rod. According to the modelling, simulation and extensive experimental results, the following conclusions are obtained:

1) The resonant frequency was 14Hz. During the frequency range of 0 to 80Hz, the peak-to-peak voltage of EH, PH and the whole HPEH exhibited the same trend and got the peak value at 14Hz. Besides, the peak-to-peak voltage of the HPEH kept higher than 30V in the range of 10-30Hz.
2) Interestingly, the connection pattern of EH and PH after the rectifier and filter circuit showed different properties. The performance of the parallel connection was more like the EH while the series connection was closer to PH.
3) The optimum matching impedance of the EH and the HPEH with the parallel connection was 1kΩ, while the PH and the HPEH with the series connection were 10kΩ. Besides, the output power of the former was much higher than the later.
4) The proposed HPEH can generate a maximum power of 80.10mW under the excitation accelerate of 2.0g at

the resonant frequency of 14 Hz with the resistance 1kΩ and the parallel connection pattern of PH and EH.

5) The HPEH can light up 120 LEDs simultaneously and power the electronics and sensors steadily, which exhibits a great potential of self-power sensing and battery-free electronics in the monitoring system of mechanical equipment in the coal mine.

REFERENCES

[1] Y. H. Chen, J. Ou, and X. Ma, "Research on coal mine safety wireless monitoring system based on Bluetooth technology," *Adv. Mater. Res.*, vols. 765–767, pp. 2061–2064, Sep. 2013.
[2] Y. Jian-jian, W. Zi-rui, T. Zhi-wei, W. Feng-dong, Z. Zhi-hua, H. Song, and W. Miao, "Intelligent recognition of cutting load of coal mining equipment based on vibration wavelet packet feature," in *Proc. 9th Int. Conf. Modeling, Identificat. Control (ICMIC)*, Jul. 2017, pp. 669–674.
[3] K. Fan, J. Chang, W. Pedrycz, Z. Liu, and Y. Zhu, "A nonlinear piezoelectric energy harvester for various mechanical motions," *Appl. Phys. Lett.*, vol. 106, no. 22, Jun. 2015, Art. no. 223902.
[4] K. Fan, Q. Tan, Y. Zhang, S. Liu, M. Cai, and Y. Zhu, "A monostable piezoelectric energy harvester for broadband low-level excitations," *Appl. Phys. Lett.*, vol. 112, no. 12, Mar. 2018, Art. no. 123901.
[5] K. Fan, L. Wang, Y. Zhu, Z. Liu, and B. Yu, "Performance of a multipurpose piezoelectric energy harvester," *Int. J. Modern Phys. B*, vol. 31, no. 07, Mar. 2017, Art. no. 1741007.
[6] M. A. Halim, M. H. Kabir, H. Cho, and J. Y. Park, "A frequency upconverted hybrid energy harvester using transverse impact-driven piezoelectric bimorph for human-limb motion," *Micromachines*, vol. 10, no. 10, pp. 701–714, Oct. 15, 2019.
[7] S. Qian, L. Qin, J. He, N. Zhang, J. Qian, J. Mu, W. Geng, X. Hou, and X. Chou, "A lead-free stretchable piezoelectric composite for human motion monitoring," *Mater. Lett.*, vol. 261, Feb. 2020, Art. no. 127119.
[8] M. Safaei, H. A. Sodano, and S. R. Anton, "A review of energy harvesting using piezoelectric materials: State-of-the-art a decade later (2008–2018)," *Smart Mater. Struct.*, vol. 28, no. 11, Nov. 2019, Art. no. 113001.
[9] X. Yuan, X. Gao, J. Yang, X. Shen, Z. Li, S. You, Z. Wang, and S. Dong, "The large piezoelectricity and high power density of a 3D-printed multilayer copolymer in a rugby ball-structured mechanical energy harvester," *Energy Environ. Sci.*, vol. 13, no. 1, pp. 152–161, 2020.
[10] Z. Yang, S. Zhou, J. Zu, and D. Inman, "High-performance piezoelectric energy harvesters and their applications," *Joule*, vol. 2, no. 4, pp. 642–697, Apr. 2018.
[11] X. G. Guo, Y. L. Zhang, K. Q. Fan, C. K. Lee, and F. Wang, "A comprehensive study of non-linear air damping and 'pull-in' effects electrostatic energy harvesters," *Energy Convers. Manage.*, vol. 203, Jan. 2020, Art. no. 112264.
[12] K. Fan, G. Liang, Y. Zhang, and Q. Tan, "Hybridizing linear and nonlinear couplings for constructing two-degree-of-freedom electromagnetic energy harvesters," *Int. J. Energy Res.*, vol. 43, no. 4, pp. 1–16, 2019.
[13] J. Siang, M. H. Lim, and M. Salman Leong, "Review of vibration-based energy harvesting technology: Mechanism and architectural approach," *Int. J. Energy Res.*, vol. 42, no. 5, pp. 1866–1893, Apr. 2018.
[14] J. He, S. Qian, X. Niu, N. Zhang, J. Qian, X. Hou, J. Mu, W. Geng, and X. Chou, "Piezoelectric-enhanced triboelectric nanogenerator fabric for biomechanical energy harvesting," *Nano Energy*, vol. 64, Oct. 2019, Art. no. 103933.
[15] W. Paosangthong, R. Torah, and S. Beeby, "Recent progress on textile-based triboelectric nanogenerators," *Nano Energy*, vol. 55, pp. 401–423, Jan. 2019.
[16] J. He, T. Wen, S. Qian, Z. Zhang, Z. Tian, J. Zhu, J. Mu, X. Hou, W. Geng, J. Cho, J. Han, X. Chou, and C. Xue, "Triboelectric-piezoelectric-electromagnetic hybrid nanogenerator for high-efficient vibration energy harvesting and self-powered wireless monitoring system," *Nano Energy*, vol. 43, pp. 326–339, Jan. 2018.
[17] K. Fan, J. Hao, Q. Tan, and M. Cai, "A monostable hybrid energy harvester for capturing energy from low-frequency excitations," *J. Intell. Mater. Syst. Struct.*, vol. 30, nos. 18–19, pp. 2716–2732, Nov. 2019.
[18] M. Renaud, P. Fiorini, R. van Schaijk, and C. van Hoof, "Harvesting energy from the motion of human limbs: The design and analysis of an impact-based piezoelectric generator," *Smart Mater. Struct.*, vol. 18, no. 3, Mar. 2009, Art. no. 035001.
[19] X. Zhang, J. Ai, Z. Ma, Z. Du, D. Chen, R. Zou, and B. Su, "Magnetoelectric soft composites with a self-powered tactile sensing capacity," *Nano Energy*, vol. 69, Mar. 2020, Art. no. 104391.
[20] Z. Li, T. Li, Z. Yang, and H. E. Naguib, "Toward a 0.33 w piezoelectric and electromagnetic hybrid energy harvester: Design, experimental studies and self-powered applications," *Appl. Energy*, vol. 255, Dec. 2019, Art. no. 113805.
[21] H. Xia, R. Chen, and L. Ren, "Analysis of piezoelectric–electromagnetic hybrid vibration energy harvester under different electrical boundary conditions," *Sens. Actuators A, Phys.*, vol. 234, pp. 87–98, Oct. 2015.
[22] Z. Xu, X. Shan, H. Yang, W. Wang, and T. Xie, "Parametric analysis and experimental verification of a hybrid vibration energy harvester combining piezoelectric and electromagnetic mechanisms," *Micromachines*, vol. 8, no. 6, p. 189, Jun. 2017.
[23] K. Fan, Q. Tan, H. Liu, Y. Zhu, W. Wang, and D. Zhang, "Hybrid piezoelectric-electromagnetic energy harvester for scavenging energy from low-frequency excitations," *Smart Mater. Struct.*, vol. 27, no. 8, Aug. 2018, Art. no. 085001.
[24] M. Iqbal and F. U. Khan, "Hybrid vibration and wind energy harvesting using combined piezoelectric and electromagnetic conversion for bridge health monitoring applications," *Energy Convers. Manage.*, vol. 172, pp. 611–618, Sep. 2018.
[25] Y. Tadesse, S. Zhang, and S. Priya, "Multimodal energy harvesting system: Piezoelectric and electromagnetic," *J. Intell. Mater. Syst. Struct.*, vol. 20, no. 5, pp. 625–632, Mar. 2009.
[26] R. M. Toyabur, M. Salauddin, H. Cho, and J. Y. Park, "A multimodal hybrid energy harvester based on piezoelectric-electromagnetic mechanisms for low-frequency ambient vibrations," *Energy Convers. Manage.*, vol. 168, pp. 454–466, Jul. 2018.
[27] H. Lin, P.-L. Hsu, T. Chen, H. Liu, H. Huang, L. Sun, and L. Cui, "Design of a hybrid piezoelectric-electromagnetic vibration power generator," in *Proc. IEEE 16th Int. Conf. Nanotechnol. (IEEE-NANO)*, Aug. 2016, pp. 464–467.
[28] H. Xia, R. Chen, and L. Ren, "Parameter tuning of piezoelectric–electromagnetic hybrid vibration energy harvester by magnetic force: Modeling and experiment," *Sens. Actuators A, Phys.*, vol. 257, pp. 73–83, Apr. 2017.
[29] G. Shi, J. Chen, Y. Peng, M. Shi, H. Xia, X. Wang, Y. Ye, and Y. Xia, "A piezo-electromagnetic coupling multi-directional vibration energy harvester based on frequency up-conversion technique," *Micromachines*, vol. 11, no. 1, pp. 80–93, 2020.
[30] Z. Zhang, C. Ni, and L. Hou, "Power generation performance of cantilever beam Bimorph in different connection modes," *Chin. J. Electron Devices*, vol. 41, no. 4, pp. 893–897, 2018.

YUN YANG received the M.S. degree in mechatronics engineering from the Harbin Institute of Technology, Harbin, China, in 2014. He is currently pursuing the Ph.D. degree in instrumentation science and technology with the North University of China, Taiyuan, China.

From 2014 to 2018, he was a Teaching Assistant with Luliang University, Lvliang, China, where he has been a Lecturer, since 2019. His main research interests include energy harvesting and online monitoring systems.

TINGTING CAI received the B.S. and M.S. degrees in metallurgy engineering from Northeastern University, Shenyang, China, in 2012 and 2014, respectively. She is currently pursuing the Ph.D. degree in material science and engineering with the North University of China, Taiyuan, China.

Since 2014, she has been a Teaching Assistant with the Department of Chemistry and Chemical Engineering, Luliang University, Lvliang, China. Her research interests include preparation of advanced functional nanomaterials their application, including piezoelectric materials, metal-containing energy-storage materials, and new carbon materials.

SHUPING XUE received the B.S. degree in chemical education from Shanxi Normal University, Linfen, China, in 1998, and the M.S. degree in inorganic chemistry from Shanxi University, Taiyuan, China, in 2006.

From 2000 to 2013, she was a Lecturer with Luliang University. She has been an Associate Professor since 2013. She was a Secretary with the Department of Mining Engineering, Luliang University, in 2019. Her main research interests include functional material preparation and energy harvesting.

XIAOGUANG SONG is currently pursuing the bachelor's degree in mechanical and electronic engineering with Luliang University, Lvliang, China. His major research interests include mechanical design and 3D printing.

XINAI CUI is currently pursuing the bachelor's degree in mechanical design, manufacturing and automation with Luliang University, Lvliang, China. Her major research interest includes simulation of mechanical structure.